Welding in the World (2023) 67:2153–2162
https://doi.org/10.1007/s40194-023-01560-0

RESEARCH PAPER

A study on creep and mechanical properties at high temperature of SMAW welds for a Cr–Mo-X steel

Sanghyun Bae[1] · **Yongchul Kim**[1] · **Stephen Liu**[2]

Received: 1 March 2023 / Accepted: 3 July 2023 / Published online: 24 July 2023

Abstract

This research describes the development of new welding materials with high strength and high heat resistance for Cr–Mo-X type steels. Alloy design of Cr–Mo-X weld metal was carried out through thermodynamic simulation. Considerations were given to the addition of chemical elements such as W that would enhance high temperature alloy stability and property enhancement. The target composition (in wt.%) for the newly designed electrodes is C: 0.10, Si: 0.27, Mn: 0.75, V: 0.25, Nb: 0.08, N: 0.02, and O: 0.05, and the welds produced using the newly designed welding electrode had excellent mechanical properties, especially in high temperature tensile testing at 600 ℃ with 385.3 MPa yield strength, 393.2 MPa tensile strength, and 23.5% elongation. Refinement of second phase particles was key to the success of the newly designed electrodes. Presence of $M_{23}C_6$ is noticeable in the new electrode welds which contributed to the high temperature strength and creep properties. Carbonitride precipitates were not detected in the welds in any major amount. Compared to conventional products, it was confirmed that in the newly designed welds, the amount of $M_{23}C_6$ precipitates, measured in area fraction, increased substantially, from 5.9 to 11.9%. *Z*-phase, known to degrade weld brittle fracture resistance, was reduced from 0.47% to 0.26% through adjusting chemical composition of the experimental welds. The welding consumable design 1 in this work is expected to allow for higher operating temperatures and higher operation efficiencies of power generation equipment in the advanced USC power plants, as well as a decrease in CO_2 emission.

Keywords Welding · Modified 9Cr-0.5Mo steel · Welding consumable for 9Cr-0.5Mo steel · Creep properties · *Z*-phase precipitates · Laves phase

1 Introduction

The demand for electricity production in the last few decades has increased progressively due to the rapid growth of the industries. There is also an increasing demand for better environmental practices in the industrial ecosystem based on IT technology [1–3].

The increase in power demand due to industrialization and continuous national economic growth has resulted in increases in energy usage and excessive emission of environmental pollutants. Since thermal power generation is recognized as the main cause of global warming, international geo-political parties have increased the speculation of restricted energy resources.

To counter the waste of the finite energy resources and decrease environmental pollution, strategies for generating power under higher temperature and higher pressure conditions have been proposed to increase power generation efficiency of power plants [2–6]. It is, thus, necessary to review and develop materials for power plants that will operate in the increasingly harsh environments with higher temperatures and pressures.

Table 1 shows that in the progression of super critical (SC), ultra-supercritical (USC) to advanced ultra-supercritical (A-USC) operating conditions, the steam temperature is expected to increase from the mid 500 °C to over 600 °C and a corresponding increase in power generation efficiency of 5%. Of equal importance, CO_2 emission would decrease

Recommended for publication by Commission II—Arc Welding and Filler Metals.

✉ Sanghyun Bae
Kisbae@kiswel.com

[1] KISWEL R&D Center, 704, Gongdan-Ro, Seongsan-Gu, Changwon-Si, Gyeongsangnam-Do, South Korea

[2] Colorado School of Mines, 1500 Illinois Street, Golden CO 80401, USA

Table 1 Steam temperature, power generation efficiency, and CO_2 generation according to the type of power plant [9]

Type	SC	USC	A-USC
Steam temp. (℃)	540/565	600/620	650/670
Power generation efficiency (%)	43	45	48
CO_2 (g/kWh)	850	750	700

from 850 g/kWh to 700 g/kWh [7–10]. Thus, operating a power plant under the A-USC conditions is highly desirable. Innovative materials and fabrication methods for power plant equipment are continuously being developed and deployed to meet the more demanding operating conditions.

This work describes the development of welding consumables for the newer steels that can perform more satisfactorily in the increasing operating temperatures, increasing operation efficiencies, and decreasing CO_2 emissions.

9Cr-1Mo-X type steel material has excellent creep properties and oxidation resistance, so it has been used as the most suitable material for power generation equipment to date [4–6, 11]. X represents additional alloying elements such as V, Nb, W, and others to enhance high temperature properties of the Cr–Mo grade steels [6–8, 10–12].

New power plant materials allow for increasing steam temperature and improved thermal efficiency. Since most of the connection parts of the power plant structures are fabricated by welding, it is very important that the development of welding materials can perform well in the selected welding processes. More importantly, the welded connections must match the performance of these advanced power plant materials. Therefore, welding electrodes with improved high-temperature properties are targets of research and development efforts.

Welding electrodes were designed in this study to improve the high-temperature characteristics of Cr–Mo-X steel welds. The performance of the welding materials was confirmed by their good creep characteristics and high-temperature properties as presented later in this work.

2 Experimental procedure

The main alloy composition of 9Cr-1Mo-V-Nb steel, which is currently a plant material for power generation equipment, is consisted of C (0.08–0.12), Mn (0.30–0.60), Si (0.20–0.50), Cr (0.00–9.50), Mo (0.85–0.05), V (0.18–0.25), N (0.03–0.07), Ni (max 0.06), Al (max 0.02), Nb (0.06–0.10), and Fe (bal.), all in weight percent [13, 15, 18].

Common design practices recommend a matching weld composition, i.e., with a chemical composition that is similar to that of the base metal [17]. Table 2 illustrates the composition of such a welding electrode. When subjected to welding and post-weld heat treatment, the deposited materials are expected to consist mainly of tempered martensite with a dispersion of oxide inclusions, Cr-rich $M_{23}C_6$, and (V,Nb)-rich MX precipitates [12, 14]. The tempered martensite, the carbides, and precipitates will develop the strength and creep properties of the welded connections.

Alloy design of the welding consumables was carried out using thermodynamic simulation (ThermoCalc® 2019a, TCFE6 v6.2) [18] to identify enhanced compositions within the standard range of commercial weld metals as defined by the AWS A5.5 E9015-B91 specification [16].

Thermodynamic modeling allowed for the determination of the major phase, which is BCC/BCT at room temperature, and the minor phases, which are oxide inclusions, carbides, and nitrides. The type and amount of inclusions and the predicted phases are shown in Table 3. *Z*-phase is defined as Cr(Nb,V)N.

For the welding experiments, 20-mm-thick P91 steel plates were used as the base material, with a joint preparation of 20° included angle and a root gap of 16 mm according to AWS A5.5 specification [16]. Shielded metal Arc welding (SMAW) was performed with a total of 18 passes in 9 layers per the schematic shown in Fig. 1. The joint surfaces were buttered prior to the deposition of the weld passes. The numbers in the schematic represent the weld deposition sequence.

The welding conditions were as follows:

Table 3 Prediction of phases (in Vol.%) present in 9Cr-1Mo(B91) using Thermo-Calc® Software [18]. Data are expressed in volume fraction

Inclusions			Matrix	
Mn_2O_2•SiO_2	MnO•Al_2O_3	MnO.Cr_2O_3	BCC/BCT	
0.21	0.01	0.17	97.02	
Precipitates				
$M_{23}C_6$	TiN	(V,Nb)N	M_2B	*Z*-phase
1.93	0.01	0.34	-	0.47

Table 2 Chemical composition (in Wt%) of weld metal for KISWEL 9Cr-1Mo welding electrode [15]. The composition was selected based on the AWS A5.5 E9015-B91 specification

C	Si	Mn	P	S	Ni	Cr	Mo	Nb
0.087	0.25	0.49	0.008	0.005	0.39	8.80	0.99	0.04

a. Welding rod size of 4.0 × 400 mm
b. Welding interpass temperature between 200 and 315 °C
c. Heat input between 13.8 and 17.9 kJ/cm
d. Post-weld heat treatment at 760 °C for 2 h

Weld metals were then analyzed for chemical composition by spark emission spectrometer and inductively-coupled plasma spectrometer (ICP) tests. The welds were also examined using standard light optical microscopy, scanning, and transmission electron microscopy together with focused ion beam (FIB) technique for their microstructures and microanalysis. Specimens were obtained for room temperature (RT) and high temperature tensile tests. Furthermore, test specimens were extracted for creep rupture testing. Visual inspection of the welds and their cross-sections showed no welding defects that would compromise the mechanical testing results.

3 Results and discussion

In this study, the weld metal was designed by thermodynamic modeling of 9Cr-1Mo-X steel to result in a desirable fine microstructure and improved high-temperature properties.

3.1 To design chemical composition of weld metal

The phase contents were clearly affected by the presence of weld oxygen, nitrogen, carbon, and niobium. Figure 2 shows the respective expected phase contents as a function of the four elements named above.

As expected, the $MnCr_2O_4$ ($MnO.Cr_2O_3$) spinel increased significantly with oxygen content. By adjusting the amounts of deoxidizers in the welding consumable, it is possible to control the amount of the oxide inclusion population. The *Z*-phase would increase to a maximum followed by a decrease with increasing nitrogen content. Given the degrading properties of *Z*-phases, nitrogen concentration should be restricted to low values.

Expectedly, increasing carbon content would increase the resulting $M_{23}C_6$ population. The presence of niobium, however, would compete for the carbon to form NbC, which would then decrease the amount of $M_{23}C_6$. Small adjustments of niobium concentration can be very useful in controlling the type and amount of second phase particles. For enhanced high temperature properties, the new ferrite-based welding consumables in this work would be developed based on the following three premises. The weld metal must contain the following:

1. Refined oxide inclusions
2. Increased fraction of fine $M_{23}C_6$ precipitates
3. Reduced amount of *Z*-phase [Cr(Nb,V)N]

By controlling the weld metal oxygen, carbon, and nitrogen content, the amounts of oxide inclusions and $M_{23}C_6$ carbides can be increased, and *Z*-phase in the welds decreased. These changes enhance the mechanical properties at both room and high temperatures [3, 6, 14, 19].

Besides the initial set of KISWEL electrode, two more sets of electrodes were developed, namely, design 1 and design 2, to address the issue of *Z*-phase (see Table 4). As such, these two electrodes have compositions slightly varied from that of the Kiswel electrode. As confirmed in Table 5, and in the conclusion of this work, *Z*-phase was reduced in the weld metal, with an expected improvement in brittle fracture avoidance.

To be able to compare with literature information, three additional sets of data were included in this work. They are the reference 1, reference 2, and reference 3 welds. Data on these reference welds were obtained from literature collected from three sets of welding consumables known for their outstanding performance. Precipitates and oxide inclusions were predicted using Thermo-Calc with the reference chemical compositions of their weld metals from

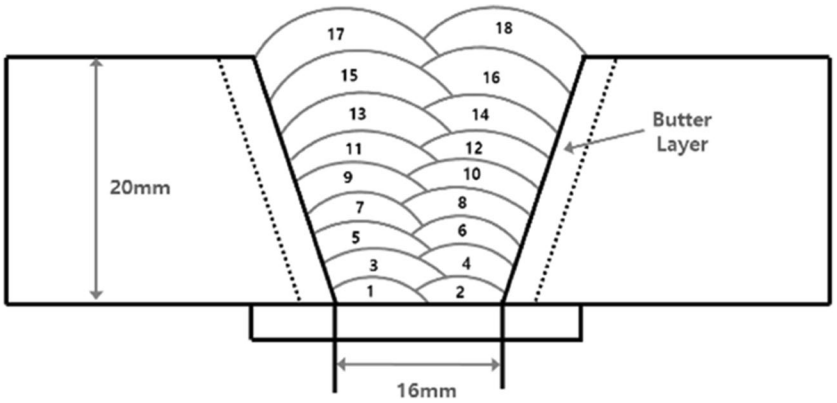

Fig. 1 The schematic of the weld deposition sequence

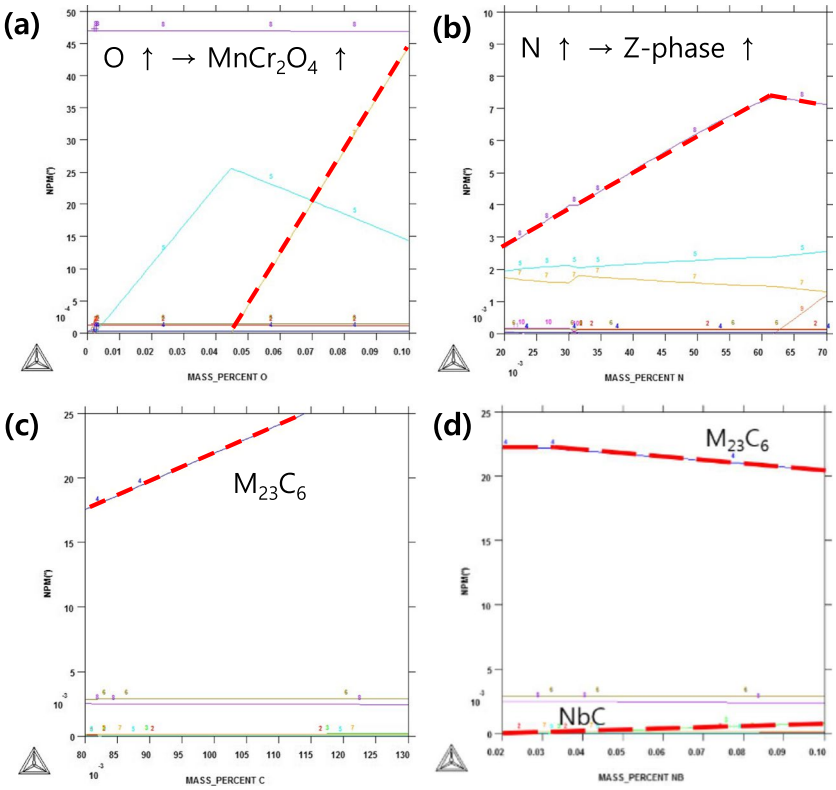

Fig. 2 Expected precipitates phase contents, $MnCr_2O_4$, *Z*-phase, and $M_{23}C_6$, according to the chemical composition (in mass percent) of (**a**) oxygen, (**b**) nitrogen, (**c**) carbon, and (**d**) niobium

Table 4 Target main chemical composition (in wt%) of weld metal of original and design 1 and 2 electrode [16]

Type	C	Si	Mn	Cr	V	Nb	N	O
Original	0.08	0.25	0.49	8.80	0.20	0.04	0.04	0.06
Design 1	0.10	0.27	0.75	8.80	0.25	0.08	0.02	0.05
Design 2	0.11	0.27	0.90	8.80	0.27	0.08	0.02	0.05

Table 5 Comparison of predicted oxide inclusions and precipitates in the KISWEL designed welds and reference welds [16]

Type	Oxide inclusion			Precipitates			
	$MnO•SiO_2$	$MnO•Al_2O_3$	M_2O_3	$M_{23}C_6$	NbC	(V,Nb)N	*Z*-phase
Original	0.21	0.01	-	1.93	-	0.34	0.47
Design 1	0.27	0.01	0.01	2.09	0.06	0.19	0.26
Design 2	0.27	0.01	0.01	1.92	0.07	0.21	0.26
Reference 1	0.32	0.01	0.00	2.36	0.03	0.32	0.42
Reference 2	0.33	0.01	0.02	2.31	0.00	0.26	0.37
Reference 3	0.24	0.01	0.01	2.19	0.02	0.23	0.28

the literature. Table 5 shows the second phase particles identified in the six sets of welds. Discussion of the results will be reported in the following sections of this work.

When compared with the reference welds, the welds made using design 1 and design 2 electrodes exhibited larger amounts of $M_{23}C_6$ phase, which is the main strengthener of the microstructure, in the absence of carbonitrides, to improve the tensile strength at room and high temperature.

Welds made using design 1 and design 2 electrodes also exhibited the lowest amounts of *Z*-phase, which is an indicator that the welds resulting from these two electrodes would experience the lowest embrittlement susceptibility.

Since all six welds would undergo post-weld heat treatment, it would be interesting to know their $\propto\rightarrow\gamma$ transformation (A1) temperature. The lower the A1 temperature, the

Table 6 A1 temperature of welds of electrode (in degrees Celsius)

A1 temperature	Original	Reference 1	Reference 2	Reference 3
	798.2	784.9	779.7	776.7

longer would be the exposure time in the γ field and more retained austenite would be present in the weld matrix [15].

Table 6 shows that the KISWEL original electrode exhibited higher A1 temperature which implies in a lower amount of retained austenite, granted that the differences of the A1 temperatures in the four sets of welds listed in Table 6 are not very large. As such, this effect of retained austenite control is not significant.

3.2 Mechanical properties and microstructures of the original 9Cr-1Mo welding consumable

Figure 3a shows the room temperature and high temperature (600 ℃) tensile test results. High temperature tensile test was performed according to ASTM E21. The weld metal performance indicated by the blue squares (both solid and open)

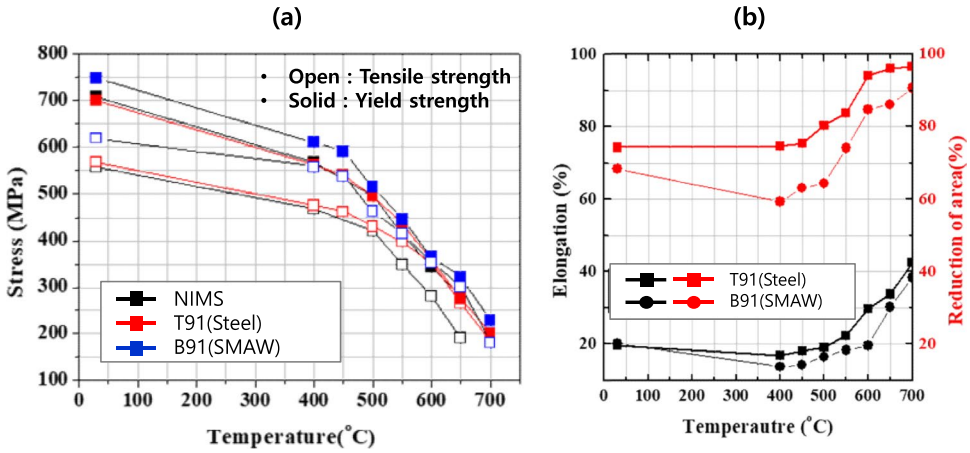

Fig. 3 Results of tensile testing of the original 9Cr-1Mo welding consumable and base metal. (**a**) Tensile and yield strength and (**b**) elongation and reduction of area. B91 (original) is the designation of the original weld

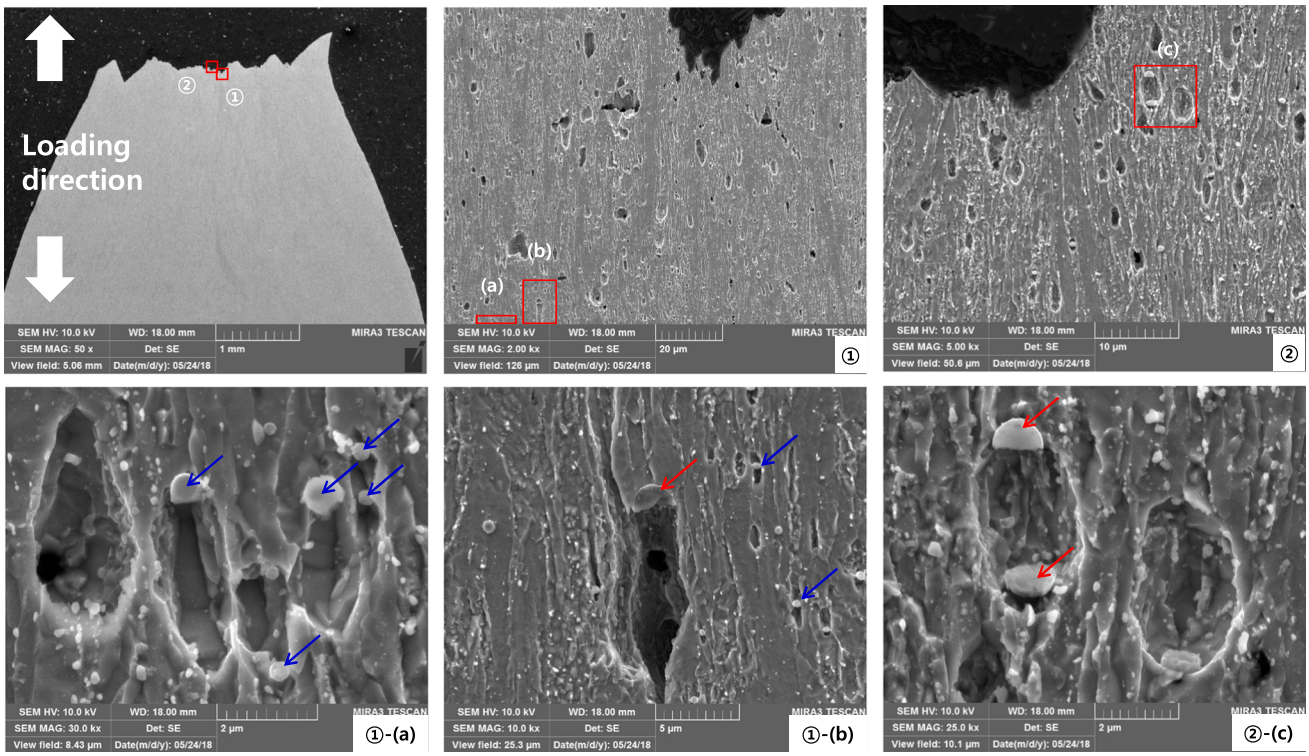

Fig. 4 SEM photographs of microvoids and inclusion after high temperature tensile test for the original 9Cr-1Mo-X weld metal

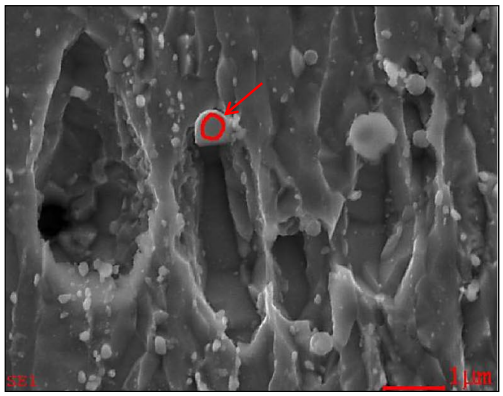

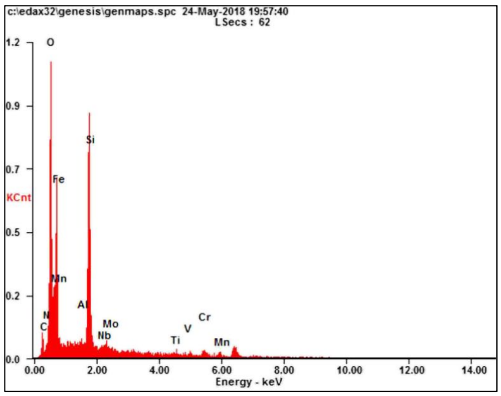

Element	Wt%	At%
C	03.89	10.12
N	01.41	03.15
O	17.08	33.39
Fe	49.29	27.61
Al	00.10	00.11
Si	17.89	19.93
Nb	00.64	00.22
Mo	01.34	00.44
Ti	01.01	00.66
V	01.04	00.64
Cr	04.37	02.63
Mn	01.95	01.11

Fig. 5 Results of EDS analysis identifying the particles as $2MnO.SiO_2$ type oxides

showed both higher yield and tensile strengths than the base metal, represented by the open and full red squares. The blue full squares represent data generated from the weld using the original electrode, labeled as B91 (original). In terms of elongation and reduction of area, Fig. 3b shows that the weld and the base metal had very similar performance. Finally, in this figure, the line with solid black squares with the NIMS label represents data reported by the Korean National Institute for Materials Science.

Microstructural observation shows elongated grains along the loading direction (Fig. 4). Oxide inclusions, as shown in Fig. 4 1-(a), 1-(b), and 2-(c), contributed to the formation of microvoids during high-temperature tensile testing.

EDS analysis of the oxide inclusions determined that they were $Mn_2O_2.SiO_2$ or $2MnO.SiO_2$ oxides, as shown in Fig. 5. These oxide particles were associated with the voids formed during mechanical testing.

3.3 Mechanical properties and microstructures of weld metal design 1 and design 2

Further characterizing and comparing the high temperature tensile properties between the three electrodes designed in this research, i.e., KISWEL original, design 1, and design 2, it can be seen in Fig. 6 that the design 1 and design 2 electrodes showed both higher tensile and yield strengths and elongation than the original electrode when tested at 600 °C. The room temperature properties of the original and designed electrodes were all superior to the reference weld. The 19.8% elongation in the design electrode 2 weld was commensurate with the 20% of the reference weld. Table 7 clearly shows that the original KISWEL electrode and the two newly designed electrodes compared very favorably against the reference electrode, with superior performance.

The fractured specimens were sectioned along the long tensile testing axis, ground flat, and polished for examination. The surface transverse to the fracture surface of the KISWEL original electrode welds and the newly designed electrodes 1 and 2 welds was examined for the determination of the number and area fraction of their oxide inclusions, as shown in Fig. 7. This figure also shows the presence of microvoids, oxide particles, and elongated grains. Oxide particles can be seen associated with the microvoids. In fact, the oxide particles likely resulted in the formation of microvoids because of the discontinuous matrix-particulate interface. The elongated grains are aligned with the tensile loading direction. Table 8 showed that the design 1 and 2 welds were cleaner (1.60×10^{-2} and $1.79\times10^{-2}/\mu m^2$) and with smaller number of oxide inclusions than the existing KISWEL products ($2.76\times10^{-2}/\mu m^2$). Furthermore, Fig. 7 shows that the inclusions in design 1 and design 2 welds were not visibly larger than those in the original electrode welds.

3.4 Creep properties

The creep test was performed according to ASTM D2209. For creep performance, the analyses were conducted

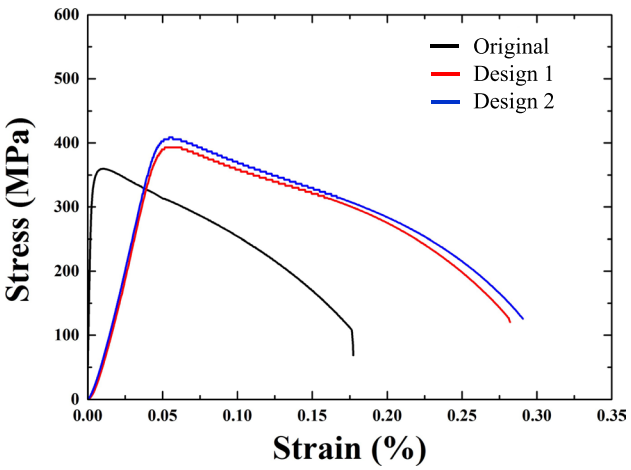

Fig. 6 Tensile test results of design 1 and 2 welds compared with original at 600 ℃

Table 7 Results of tensile test at R.T and high temperature. The dark triangles represent increase or decrease when compared with the reference weld data

Type	RT			600 ℃		
	Y.S (MPa)	T.S (MPa)	EL. (%)	Y.S (MPa)	T.S (MPa)	EL. (%)
Reference	≥600.0	≥710.0	≥20.0	≥260.0	≥370.0	≥18.0
Original	619.6	749.3	21.5	354.0	366.5	20.8
Design 1	648.8 (▲4.7%)	775.0 (▲3.4%)	21.6 (▲0.5%)	385.3 (▲8.8%)	393.2 (▲7.3%)	23.5 (▲13.0%)
Design 2	669.2 (▲8.0%)	792.9 (▲5.8%)	19.8 (▼7.9%)	390.5 (▲10.3%)	408.9 (▲11.6%)	22.9 (▲10.1%)

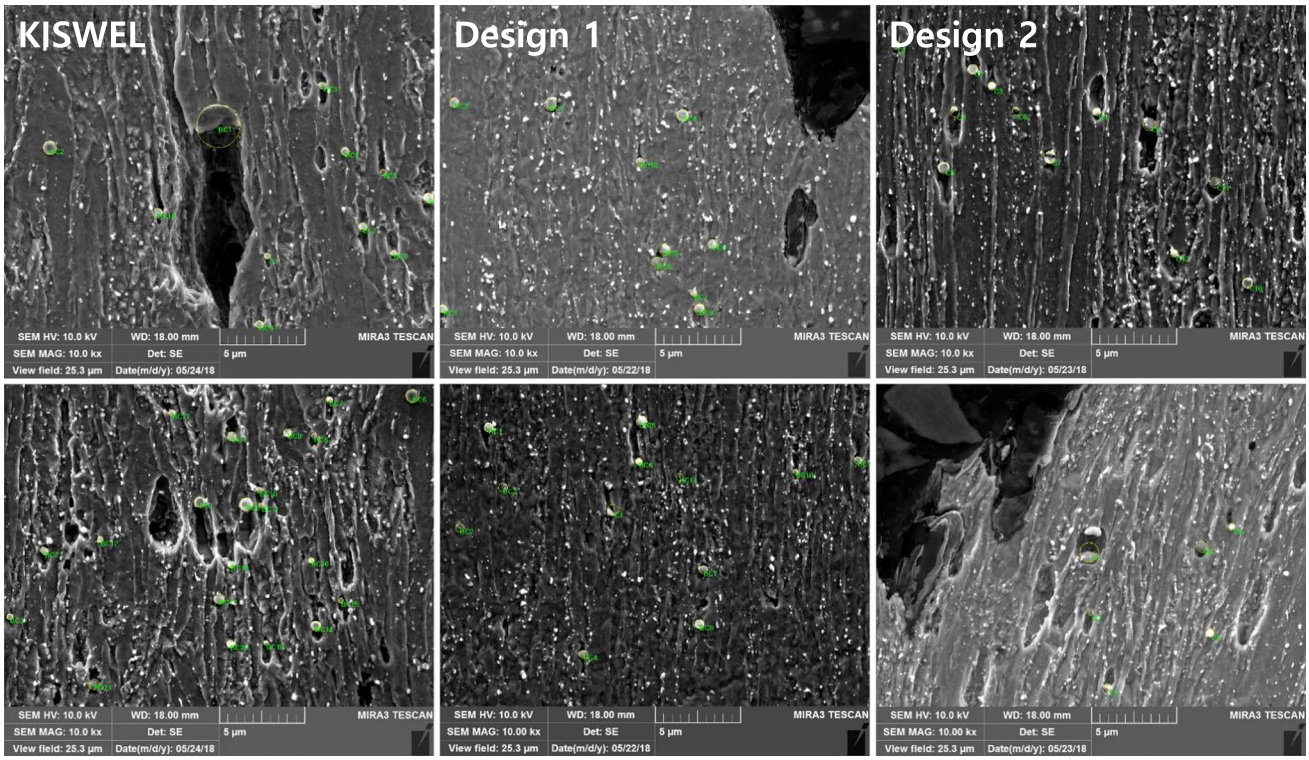

Fig. 7 SEM photographs of the cross-sectional region adjacent to the fracture surfaces of tensile tested 9Cr-1Mo-X weld metal specimens at 600 ℃ showing microvoids, oxide particles, and elongated grains

according to the Larson-Miller parameter approach as shown in Fig. 8. The creep rupture behavior of base steel and weld is summarized as a function of the applied stresses and Larson-Miller parameter (LMP) (Table 9).

$$\mathrm{LMP} = T\left[\log(t) + 25\right]$$

In this equation, T is temperature in degrees Kelvin and t is time in hours. The number 25 can be considered as a material-related constant.

The weld metal data (represented by the star symbols) in Fig. 8 were mostly on or above the base metal performance line, which means the weld metal developed in this work performed mostly better than the base metal.

It is known that creep properties of Cr–Mo-X weld joints are determined by type IV cracking. Nevertheless, the initial focus of this work was to develop a consumable that would weld the high temperature and high resistance steels with improved properties. Both objectives were achieved. Moving forward, the research program may examine the fracture

Table 8 Oxide inclusion populations in the welds produced using the KISWEL original electrode and the design 1 and design 2 electrodes

Oxide inclusion	KISWEL (Original)	Design 1	Design 2
Average area fraction (μm^2)	0.18 ± 0.11	0.21 ± 0.08	0.23 ± 0.09
Number (μm^2)	2.76	1.79	1.60

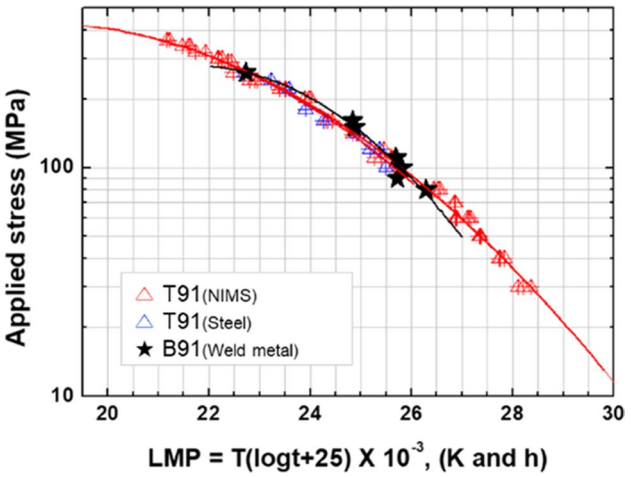

Fig. 8 Larson-Miller parameter analysis. NIMS stands for Korean National Institute for Materials Science

Table 9 Stress level and temperature of creep test

Condition of creep test for weld metal (design 1)			
Temp (℃)	550	600	650
Stress (σ) in MPa	260	180	110
	240	160	100
	230	150	90
	210	145	80
	200	130	70

of the weld joint in the ICHAZ during service or prolonged creep test [22, 23].

TEM analysis was performed to analyze the relationship between the behavior of the high-temperature tensile test and the precipitates found in the Cr–Mo-X Steel. Figure 9 shows the distribution of precipitates in focused ion beam (FIB) extracted specimens (Fig. 9a and e) from under the fracture surface of high-temperature tensile specimens and also TEM–EDX mapping and selected area electron diffraction (SAED) patterns for the characterization of the precipitates.

In SEM mapping (Fig. 9b and f) and SAED pattern (Fig. 9c, d, and g), the precipitates in both specimens were identified as similar. They were Cr-rich $M_{23}C_6$ precipitates, represented in pink (Fig. 9c and g) and (V,Nb)-rich MX precipitates (Fig. 9d) and represented in blue-green. Carbonitride precipitates were not detected in the TEM analyzed FIB sections.

Figure 10 presents the precipitates data in the weld specimens. The bar charts with the "Original" designation can be compared with the designed electrode 1 data. Figure 10a compares the MX population, and Fig. 10b compares the $M_{23}C_6$ population. The MX phase in the design 1 electrode weld was observed to slightly reduce to 0.8% area fraction. The number of MX remained almost constant but the radius of the particles decreased from 24 to 19 nm.

Figure 10b clearly illustrates the much larger population of $M_{23}C_6$ in the design 1 electrode welds. The area fraction of the $M_{23}C_6$ carbide increased from 5.9 (original) to

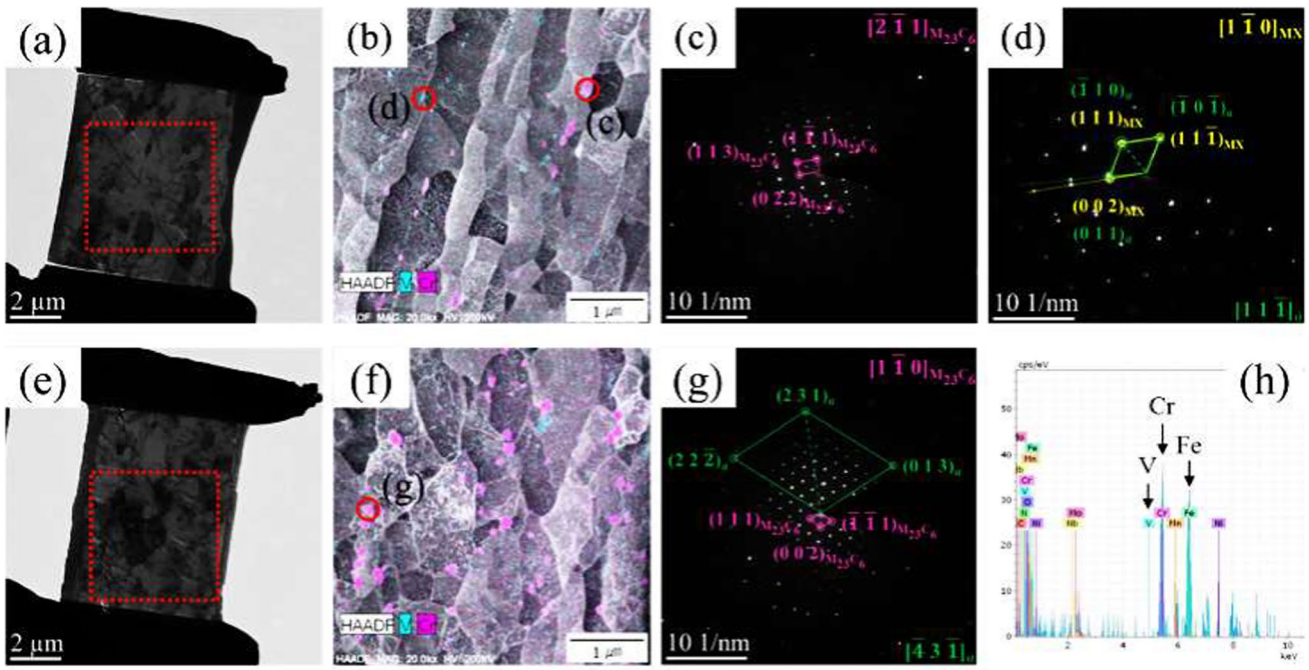

Fig. 9 TEM analysis of the cross-sectional region adjacent to the fractured surfaces of tensile tested 9Cr-1Mo-V-Nb weld metal specimens at 600 ℃: (**a**) FIB section, (**b**) SEM mapping, (**c**, **d**) SAED pattern of particle shown in (**b**) of 0.09C, (**e**) FIB section, (**f**) SEM mapping, (**g**) SAED pattern of particle shown in (**f**) of 0.10C, and (**h**) Cr-rich $M_{23}C_6$ X-ray spectrum

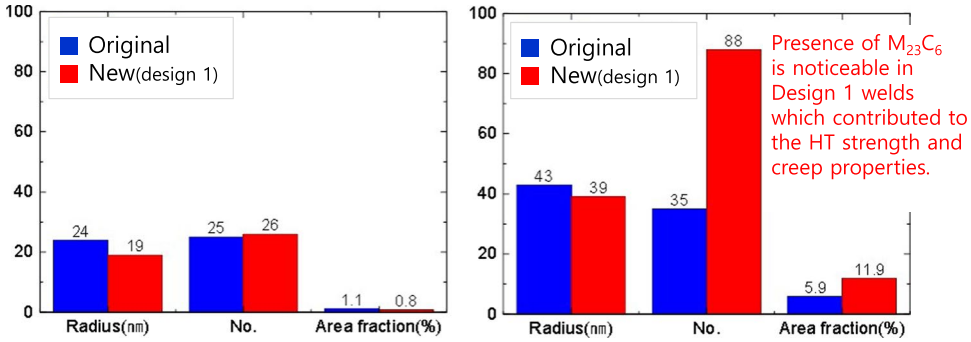

Fig. 10 Area fraction of (**a**) MX-phase and (**b**) $M_{23}C_6$ carbide

11.9%, while the number of carbide particles extracted was 88 as compared to 35 (original). These numbers imply in a more significant contribution of these precipitates to the high temperature strength of the weld, particularly after the post-weld heat treatment cycle. The radius of the carbide particles decreased from 43 to 39 nm.

Post-weld heat treatment affects the kinetics of formation and growth of the Laves phase as evidenced in Fig. 11. Note the appearance and growth of the Laves particles with time, from 3,717 h to 11,615 h when subjected to creep condition of 600 °C and 140 MPa. As Laves phase negatively impacts the mechanical properties of welds, this research shows that the designed electrode 1 had only 0.70% Laves phase, as compared with 0.99% formed in the original (Kiswel) electrode weld. From the reference welds, Laves phase as high as 1.05% was found. As such, design 1 electrode was able to keep the amount of Laves phase to a very low level [23].

Table 10 summarizes the second phase particles data. Welds from design 1 electrode exhibited the best inclusions and precipitates population when compared with the original and reference electrodes, with 0.47% oxide inclusions, 2.46% $M_{23}C_6$, 0.7% Laves phase, and 0.43% *Z*-phase. While the increase in $M_{23}C_6$ indicates improved high temperature properties, the decreases in Laves phase and *Z*-phase point to greater resistance in embrittlement [19–23].

4 Conclusion

New consumables are needed to produce acceptable high temperature properties to match those developed for newer materials used in advanced power plant equipment. The conclusions of this research can be summarized below:

A) Thermodynamic modeling was able to assist in the development of welding electrodes for Cr–Mo-X steels that improved high temperature properties
B) The design 1 and 2 electrodes produced welds that exhibited greater tensile and yield properties, and elongation at room temperature and 600 °C than welds produced by reference electrodes
C) Larson-Miller parameter analysis of HT behavior of the newly designed weld metals showed properties com-

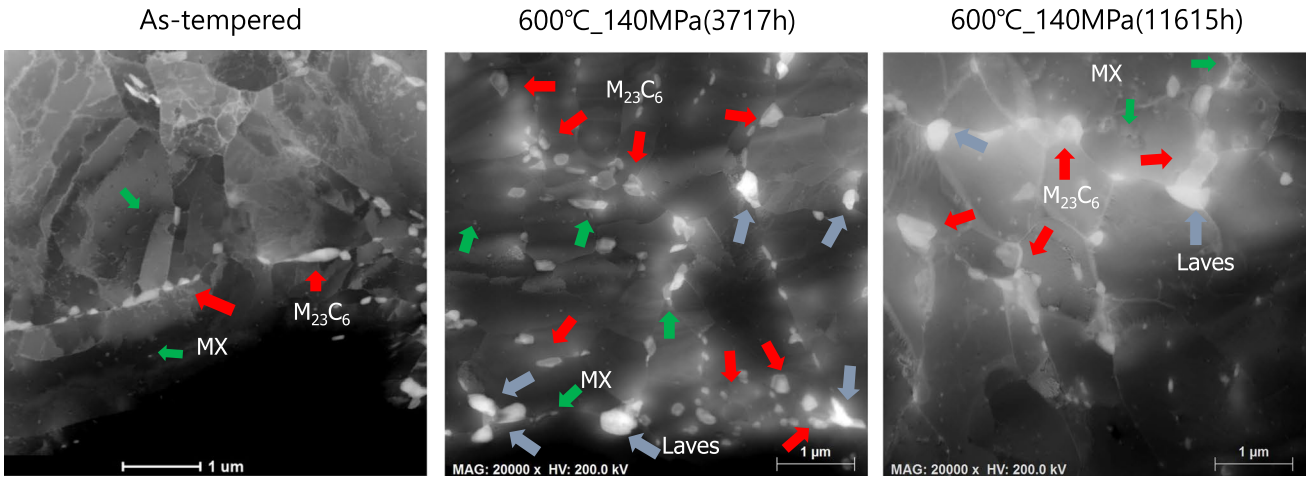

Fig. 11 Appearance and growth of Laves phase precipitates during and after post-weld heat treatment. Both temperature and time are required for the growth of Laves phase [19]

Table 10 Prediction of phase present in design 1 compared to reference 1, 2, and 3 using Thermo-Calc® Software

Type	Oxide inclusion			Precipitate		
	$Mn_2O_2•SiO_2$	$MnO•Al_2O_3$	$MnCr_2O_4$ (spinel)	$M_{23}C_6$	Laves	*Z*-phase
Original	0.46%	0.01%	-	2.15%	0.99%	0.56%
Design 1	-	0.01%	0.46%	2.46%	0.70%	0.43%
Reference 1	0.43%	0.01%	-	2.13%	0.86%	0.64%
Reference 2	-	0.01%	0.56%	2.09%	1.05%	0.46%
Reference 3	0.23%	0.01%	-	1.54%	0.88%	0.67%

parable to those required for the advanced power plant materials

D) The design 1 electrode produced a smaller amount of oxide inclusions but a larger amount of $M_{23}C_6$ precipitates than the original electrode weld, which is proper for the development of better high temperature properties

E) The design 1 electrode produced reduced amounts of *Z*-phase and Laves phase precipitates which implies in diminished embrittlement susceptibility

F) The newly designed weld metal will satisfy the higher operating temperature and efficiency of the power plant equipment with expected decreases in CO_2 emission

Declarations

Conflict of interes The author declares that there exists no competing financial interest or personal relationships that could have appeared to influence the work reported in this paper.

References

1. Kupzog Ove F, King R, Stefan M (2020) The role of IT in energy systems: the digital revolution as part of the problem or part of the solution. Elektrotechnik und Informationstechnik 137:341–345
2. Abe F, Tabuchi M (2004) Microstructure and creep strength of welds in advanced ferritic power plant materials. Sci Technol Weld Joining 9(1):22–30. https://doi.org/10.1179/136217104225017107
3. Abe F (2008) Heat-to-heat variation in long-term creep strength of some ferritic steels. Sci Technol Adv Mater 9(013002):310–318
4. David SA, Seifert JA, Feng Z (2013) Welding and weldability of candidate ferritic alloys for future advanced ultrasupercritical fossil power plants. Sci Technol Weld Joining 18(8):631–651. https://doi.org/10.1179/136217183Y.0000000152
5. Lomozik M, Zeman M, Brózda J (2012) Modern martensitic steels for power industry. Arch Civil Mechanical Eng 12:49–59
6. Maruyama K, Sawada K, Koike J (2001) Strengthening mechanisms of creep resistant tempered martensitic steel. ISIJ Int 41:641–653
7. Bedick W, Gabrel J, Hahn B, Vandeberghe B (2007) New alloy heat resistant ferritic steels T/P23 and T/P24 for power plant application. Int J Press Vessels Pip 84:13–20
8. Hilkes J and Gross V (2013) Welding CrMo steels for power generation and petrochemical applications _ Past, Present and Future, Böhler Schweisstechnik Deutschland GmbH, 10 pp,
9. Gianfrancesco AD (2017) Gianfrancesco, Materials for ultra-supercritical and advanced ultra-supercritical power plants, pp. 8–13, Woodhead Publishing, Italy
10. Sorrentino S (2017) Welding technologies for ultra-supercritical power plant materials, in Materials for Ultra-Supercritical and Advanced Ultra-Supercritical Power Plants, pp. 247–319. https://doi.org/10.1016/B978-0-08-100552-1.00009-9
11. Swindeman RW, Santella ML, Maziasz PJ, Roberts BW, Coleman K (2004) Issues in replacing Cr-Mo steels and stainless steels with 9Cr-1Mo-V steel. Int J Pres Ves Pip 81:507–512
12. Young GA, Capobianco TE, Etien RA, D'Amore LL, Sander PC, Schmidt K, Sutliff JA, Sham KL and Liu S (2008) "Development of a highly weldable and corrosion resistant nickel-chromium filler metal for use in nuclear power systems," presented and published in the 8th International EPRI Conference on 'Welding and Repair Technology for Power Plants', Paper 2A-03, EPRI-1018070, Fort Myers, Florida.
13. Hashimoto T, Tanaka Y, Hokano M, and Hirasaki D (2008). "Latest technology of highly efficient coal-fired thermal power plants and future prospects," Mitsubishi Heavy Industries Technical Review, Vol.45 ,No.1, page 11- 14, Japan
14 Arivazhagan B, Vasudevan M (2015) Studies on A-TIG welding of 2.25Cr-1Mo (P22) steel. J Manuf Process 19:55–59
15. Kiswel RD (2020) Design of arc welding consumables for Cr-Mo-X steels for advanced power generation equipment
16. American Welding Society, Specification for low-alloy steel electrodes for shielded metal arc welding, AWS A5.5/A5.5M p8–9
17. Liu S (2008) "Revisiting the effects of undermatching and overmatching on weld hydrogen pickup and mitigation through design of advanced consumables," in the Proceedings of the International Masao Toyoda Symposium – From Welding and Fracture Mechanics to Pipeline Technology, pp. 65–80, Osaka, Japan, June 28–29
18. Thermo-Calc[R], ThermoCalc 2019, TCFE Database
19. Pandey C, Giri A, Mahapatra MM, Kumar P (2017) Characterization of microstructure of HAZs in as-welded and service condition of P91 pipe weldments. Met Mater Int 23:148–162
20. Syed Ghazi Sarwat, Joysurya Basu (2019) Understanding Laves phase precipitation induced embrittlement of modified 9Cr-1Mo steel, SN Applied Sciences 1(1)
21. Gianfrancesco AD, Vipraio ST and Venditti D (2013) Long term microstructural evolution of 9–12% Cr steel grades for steam power generation plants, 55: pp. 27–35, Procedia Engineering
22. Francis JA, Mazur W, Bhadeshia HKDH (2013) Review type IV cracking in ferritic power plant steels. Mater Sci Technol 22(12):1387–1395. https://doi.org/10.1179/174328406X148778
23. Francis JA, Mazur W, Bhadeshia HKDH (2004) Estimation of type IV cracking tendency in power plant materials. ISIJ Int 44(11):1966–1968